Journal Name

ARTICLE

Ideal Porous Structure of EDLC Carbon Electrode with Extremely High Capacitance

K. Urita,[a*] C. Urita,[a] K. Fujita,[a] K. Horio,[b] M. Yoshida[b] and I. Moriguchi[a]

We propose an ideal porous structure of carbon electrodes for electric double-layer capacitors (EDLCs). The porous carbon successfully improved the gravimetric capacitance above ~200 F/g even in an organic electrolyte by utilizing carbon nanopore surface more effectively. High-resolution transmission electron microscope images and X-ray diffraction patterns classified 15 different porous carbon electrodes into slit-shape and worm-like-shape, and the pore size distributions of the carbons were carefully determined using a Grand Canonical Monte Carlo method to N_2 adsorption isotherms at 77 K. The ratio of pores where solvated ions and/or desolvated ions can access has also a significantly effect on the EDL capacitance as well as the pore shape. The detail study on the effect of porous morphologies on EDLC performance indicates that a hierarchical porous structure with worm-like shape surface and the pore size ranging from a solvated ion to a solvent molecule is an ideal electrode structure.

Introduction

Electric double-layer capacitor (EDLC) has attracted significant attention due to applying to high power density and stable energy storage devices. And also, to meet the needs of recent development of portable, flexible and wearable electric devices, flexible supercapacitors have been strenuously studied[1-3]. The EDL capacitance is proportional to the electrode surface area and inversely proportional to the thickness of EDL; porous conductive materials with high surface area are desired materials as an electrode for EDLCs[4]. Although microporous carbon electrodes with higher specific surface area are expected to provide higher EDL capacitance, the micropores have been considered not to make a significant contribution to the EDL capacitance. Solvated electrolyte ions in bulk organic solution are larger than the micropore size of <1.5 nm; the solvated ions cannot access into the micropores. The customary opinion has led mesoporous carbons whose average pore size is from 2 to 50 nm to have an ideal structure as EDLC electrodes[5]. On the other hand, studies on focusing phenomena in micropores suggest that such narrow space provides a peculiar field different from bulk phase against introduced molecules. Ohkubo et al. reported that the spatial restriction of micropores causes a change in molecular coordination: a partial dehydration of ions is occurred in the micropores of porous carbons[6, 7]. Such micropores also work as a high-pressure field

whose effect has been called quasi-high pressure effect[8-12]. The unique phenomena in confined nanospcaces have been observed in electrodes for EDLCs. Some systematic studies suggest that micropores whose pore size is close to a bare ion size should work effectively to improve a specific EDL capacitance[13, 14]. An advanced study by Chmiola et al. implied initially that accessibility of electrolyte ions into micropores was increased by the partial desolvation of electrolyte ions by using quaternary ammonium ion as an electrolyte ion[13]. The possibility of desolvation in micropores has been mentioned by theoretical studies and in-situ measurements[15-21]. Such desolvation has been also occurred even on Li ions, which have high solvation energy. Our group determined the desolvation number of Li ions in micropores, mesopores, and macropores and/or on external surface of porous carbons from Raman spectra and ^{7}Li NMR spectra[22]. The solvation number is dramatically decreased in micropores, and the porous carbons with low solvation number show high area-specific capacitances. Our findings suggest that porous carbon electrodes designed based on Li-ion electrolytes should be directly applicable to a lithium-ion hybrid capacitor. From the study of area-specific capacitance relative to average pore size, the micropores are predictably effective as a space improving the capacitance[23-25]. However, the gravimetric capacitance has not been high on all of micro/mesoporous carbons showing high area-specific capacitance[26-30]. Designing a carbon electrode of high gravimetric capacitance EDLC requires knowledge not of the average pore size but also of the pore size distribution (PSD) and the pore shape. In this study, we investigated in-depth relationship between porous structures and EDL capacitances to clarify the porous structures achieving extremely high EDL capacitance. As mentioned by previous studies[31, 32], understandably, various functional groups on carbon surface may also contribute to EDL capacitances. Nevertheless, our

a. Graduate School of Engineering, Nagasaki University, 1-14 Bunkyo-machi, Nagasaki, Nagasaki 852-8521, Japan.
b. MicrotracBEL Corp., 8-2-51 Nankohigashi, Suminoe-ku, Osaka 559-0031, Japan.

finding based on the PSDs will be helpful to design an ideal porous structure because porous structure seems to be a more dominant factor than the functional groups in the case of the organic electrolyte[32]. We used 15 different activated porous carbons with different PSDs and pore shapes to systematically clarify the effect of PSDs and shapes on EDL capacitances. It should be noted because EDL is formed on the electrode surface, the PSDs were defined by the related distribution of pore area. Our findings offer detail insights into a favourable porous structure of carbon electrodes to enhance the EDL capacitance from the view point of the PSDs and shapes against solvated and/or desolvated electrolyte ion.

Experimental

Synthesis of porous carbon materials

Each porous carbon sample used here was tentatively named as T1–carbon for a phenolic resin carbon, Ax– and Wy–carbon (x: 1–4, y: 1, 2) for pitch type carbons, CHz–carbon (z: 1–3) for organic-inorganic polymer derived carbons, Mw–carbon (w: 1–3) for activated petroleum cokes and PorCt (t: 18, 45) for SiO$_2$ opal-templated carbons. The T–type is a commercial carbon produced by Futamura Chemistry Co., Ltd. The A– and W–types kindly supplied by Ad'All Co., Ltd. are well-known as activated carbon fibers (ACFs) with slit-shape pores. The ACFs were produced by different activation degrees. M–type carbons are KOH activated carbons named as Maxsorb kindly supplied by MC Evolve Technologies Co. The M3 carbon was provided by a similar activation method with the Maxsorb series. The others were synthesized as following methods. The CH-type was synthesized from an organic-inorganic hybrid polymer consisting of a phenolic part and a siloxane part (COMPOCERAN, kindly supplied by Arakawa Chemical Industries, Ltd.). A SiO$_2$ content of CH$_1$, CH$_2$ and CH$_3$ after a curing reaction is 40, 60 and 70 wt%, respectively. The SiO$_2$ has an effect on the pore sizes. They formed gels in ethanol solution by adding aqueous HCl and stirring for 48 h, and then the gels were heated at 443 K for 6 h in air and at 1273 K for 5 h under Ar gas[33]. The SiO$_2$ in the obtained SiO$_2$/C nanocomposites was removed by HF to yield porous carbons. The PorC-type was produced by a templated method. Each SiO$_2$ particle with the diameter of 18 and 45 nm dispersed in basic solution was used as a template material. The colloidal solution was centrifuged, and the supernatant solution was removed. Residual SiO$_2$ blocks were dried to form an opal structure and then immersed in phenol-formaldehyde solution added aqueous HCl for 12 h. After the same procedure with the CH-type, the PorC-type with the pore size corresponding to SiO$_2$ particle size was provided[34].

Microstructural characterization

The carbon frameworks of porous carbons were directly observed by using a high-resolution scanning transmission electron microscope (ARM-200CF, JEOL Ltd.) under transmission mode and a transmission electron microscope (JEM2010, JEOL Ltd.) at the accelerating voltage of 120 kV. Each porous carbon sample was dispersed in highly-pure ethanol

(Primepure, Kanto Chemical Co., Inc.) and then dropped on a Cu mesh covered with carbon membranes (NS-C15, Okenshoji Co., Ltd.). The spread of 2D-pore walls was confirmed by X-ray diffraction (XRD; Miniflex600-DX, Rigaku Corp.) measurements equipped with Cu Kα. Each (10) plane size was determined from Scherrer's equation. The in-plane defects were additionally confirmed from an intensity ratio of D-band to G-band (I_D/I_G) in Raman spectra measured with a Raman spectroscope (RMP-210, JASCO) with the laser excitation wavelength of 532 nm. The porosities were determined from N$_2$ adsorption isotherms at 77 K (BELSORP-max, Microtrac-bel Corp.). The N$_2$ adsorption isotherms were carefully measured from the relative pressure on the order of 10^{-8}, corresponding to pore size of ~ 0.35 nm. All adsorption isotherms were measured after pretreatment under vacuum at 423 K for 5 h.

Electrochemical analysis

EDL capacitances were determined from electrochemical charge/discharge curves measured in a sealed three-electrode glass cell with an electrochemical analyser (HJ-SD-8, Hokuto Denko) at room temperature. We used metallic Li foil on Ti meshes as a counter electrode (15 x 18 mm^2) and a reference electrode (8 x 18 mm^2), and 1 M LiClO$_4$/propylene carbonate (PC) solution was used as electrolyte solution. Previous studies reported that a theoretical desolvation energy of Li ion to PC was 218 kJ/mol[35], and the interaction of a Li ion with PC was higher than that of a tetraethylammonium (TEA) ion with PC[36], which has been widely used for EDLC studies. Because the desolvation requiring high energy should be pronouncedly occurred in micropores where introduced ions undergo a strong confinement effect, the Li-PC system is expected to be a good probe to understand the effect of porous structures on improvement of EDL capacitances. The porous carbon samples were mixed with PTFE at a weight ratio of 92:8 and then pressed onto the Ti mesh as a working electrode (15 x 18 mm^2). The average loading amount and size of porous carbon samples were 7 mg and 10 x 10 mm^2, respectively. The charging and discharging were carried out in constant current (CC) mode. The current density and the potential range were set from 10 to 500 mA/g and 2–4 V vs. Li/Li$^+$, respectively. Cyclic voltammetry (CV) measurements were also carried out using an electrochemical workstation (Solartron analytical 1470E) at a scanning rate of 1 mV/sec in the voltage range of 2.0–4.0 V.

Results and discussion

We group the porous carbon electrodes by slit-shape and worm-like (WL)-shape framework, and a mesoporous carbon from high-resolution transmission electron microscope (HR-TEM) images (Figure 1). From the carbon walls constructing pores a part of which are highlighted by red, the T-type carbon shows an intricate carbon framework because micropores below ~0.8 nm should be dominant pores, as described later (see Supplementary Information Fig. S2). The A-type and W-type carbons have wide horizontal carbon walls, which have been well-known as a micrographite, being classified into the
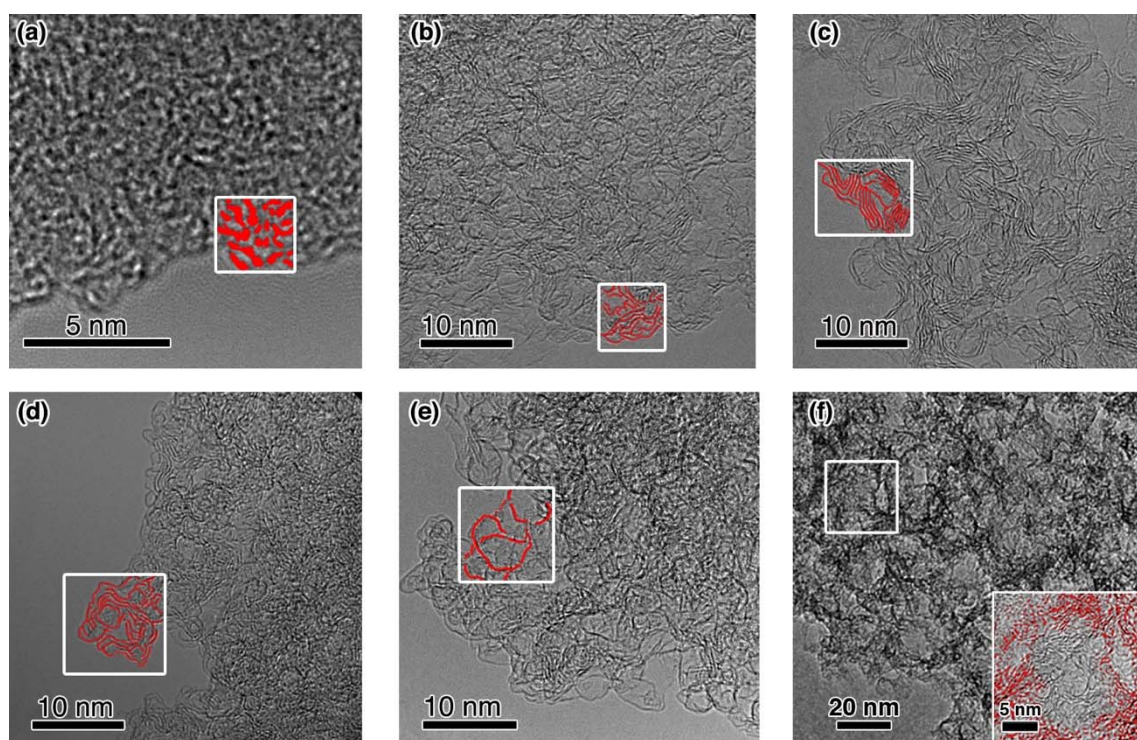
Figure 1. HR-TEM images of carbon frameworks of representative porous carbon samples. (a) T-type, (b) A-type, (c) W-type, (d) CH-type, (e) M-type and (f) PorC-type. Inset TEM image in (f) is a magnified image in a white box area. Red highlights in the white boxes show carbon walls constructing pores.
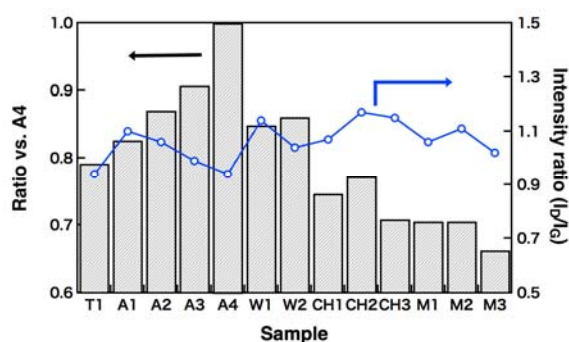

Figure 2. Ratio of (10) crystallite size against the A4 carbon with largest (10) crystallite size and intensity ratio (I_D/I_G) of micro and/or mesoporous carbons.
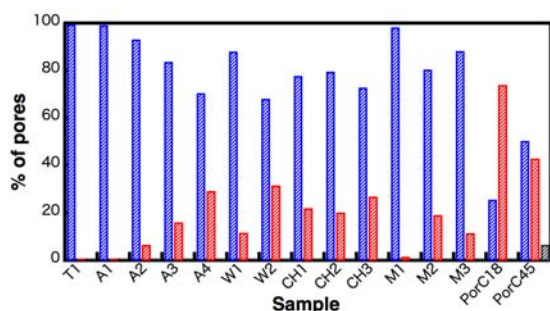

Figure 3. Percentage of micropore (blue), mesopore (red) and macropore/external (black) surface area in each sample. The percentage was determined from integration of the surface area in each pore range calculated from a GCMC method.

slit-shape. The CH-type and M-type carbons show crooked carbon walls. We named a pore shape consisting of the crooked carbon walls as WL-shape. The HR-TEM image of PorC18 (Fig. 1(f)) shows spherical pores with the pore size of ~18 nm; PorC

has mesopores with pore size reflecting the size of the templated SiO$_2$ nanoparticles.

The difference of 2D-framework size between the slit-shape carbons and the WL-shape carbons is also mentioned from a crystallite size of (10) plane determined from the XRD patterns (see Supplementary Information Fig. S1). The ratio of crystallite size of each type of micro and/or mesoporous carbon samples was defined as the ratio to the A4 carbon with the largest (10) plane, and an intensity ratio of D-band to G-band (I_D/I_G) was determined from Raman spectra (Figure 2). The T-type, A-type and W-type carbons have relatively large flat surfaces. The T-type carbon with wide (10) plane is here treated as the slit-shape carbon. The CH-type and the M-type samples obviously have smaller size of (10) plane than others, indicating that their carbons should be constructed mainly by crooked carbon frameworks. The I_D/I_G ratio is one of parameters reflecting the amount of in-plane defects in carbon materials[37-39]. Such defects are easily terminated by –OH or –COOH groups like a graphene edge[40]; the larger I_D/I_G ratio is, the more functional groups form in the carbon samples. Without distinct difference of the I_D/I_G ratio on porous carbons, they seem to have a similar amount of defects.

A percentage of surface area of micropores (pore size: $w \leq 2$ nm), mesopores ($2 < w \leq 50$ nm) and macropores/external surface ($w > 50$ nm) was determined from PSDs (Figure 3). The PSDs were carefully calculated by using a Grand Canonical Monte Carlo (GCMC) method[41] to N$_2$ adsorption isotherms at 77 K (see Supplementary Information Fig. S2 and Table S1 for the numerical data of surface area). The percentage of pores categorized by IUPAC definition clearly reveals the porosities of carbon samples. The T1, A1 and M1 carbons have a large
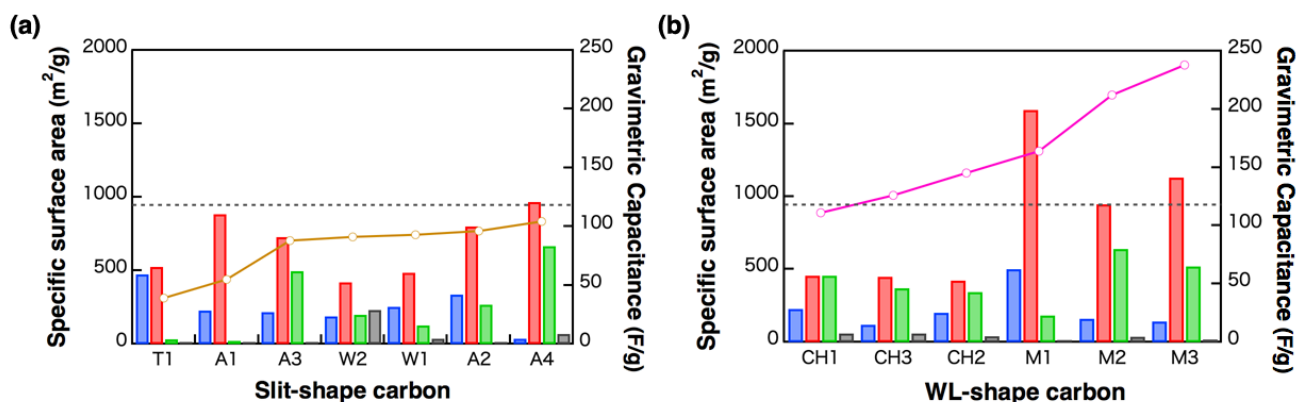
Figure 4. Specific surface area with pore size of < 0.55 nm (blue), 0.55–1.5 nm (red), 1.5–3.0 nm (green) and > 3.0 nm (black) and gravimetric capacitance at the current density at 10 mA/g (ocher in (a) and pink in (b)) on the slit-shape carbon (a) and WL-shape carbon (b). Grey short-broken lines reveal the gravimetric capacitance (118 F/g) of PorC18.
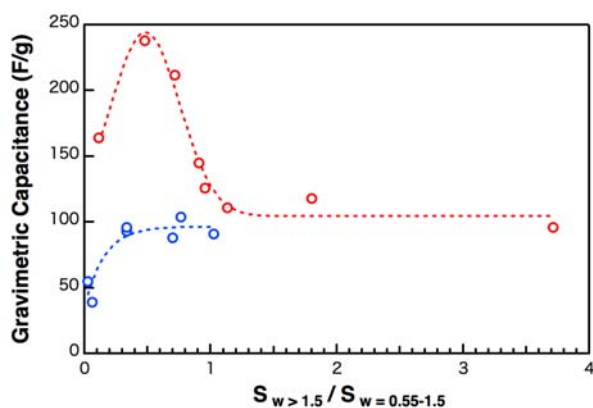

Figure 5. Gravimetric capacitance against ratio of the value of specific surface area (R_{ssa}: S_w>1.5 / S_w=0.55–1.5) on the slit-shape carbon (blue) and the WL-shape carbon and PorCs (red).

amount of micropore volume. Because the percentage of mesopore and macropore/external surface is < ~3 %, they are undoubtedly a microporous carbon. The PorC18 and 45 have a large amount of mesopores volume; PorC-type is a mesoporous carbon. Other carbons do not have macropores but are constructed by micro and mesopores; they are grouped into a micro/mesoporous carbon.

The electrochemical properties of the provided carbons were investigated by CV and galvanostatic charge/discharge measurements. The CV curves of slit-shape carbons show rectangular-shape in the slit-shape carbons and slightly butterfly-shape in the WL-shape carbons due to the charging-discharging of EDL without specific redox peaks (See Supplementary Information Fig. S3). Previous reports suggests that the butterfly-shape curves stem from the ion penetration into nanopores[42, 43]. It can be said that the effect of pseudo capacitance of functional groups is negligibly small on the EDL capacitances. The gravimetric EDL capacitances were calculated by using the galvanostatic third discharge curve at the current density of 10 mA/g (see Supplementary Information Fig. S4) below the open circuit voltage where Li ions form EDL on the electrode surfaces. The gravimetric capacitance of the WL-shape carbon (Fig. 4(b)) is higher than that of the slit-shape carbon (Fig. 4(a)). Each gravimetric capacitance of PorC18 and

PorC45 is 118 and 96 F/g, respectively. For comparison, the value of PorC18 is illustrated by grey short-broken line in Fig. 4. The WL-shape carbons also provide higher area-specific capacitance than the slit-shape carbons and the PorCs (see Supplementary Information Fig. S5). The high area-specific capacitance obviously indicates that the WL-shape pores are quite effective in EDL formation. The advantage of WL-shape carbon was also confirmed at higher current density (see Supplementary Information Fig. S6). The gravimetric capacitance of WL-shape carbons shows relatively good rate performance and is higher than that of other carbons even at high current density. It indicates that the WL-shape pore is totally effective to enhance the EDL capacitance as mentioned in previous reports[44, 45]. For in-depth understanding of porous structural effect, the specific surface area was divided into 4 domains of pore size (w), (i) w < 0.55 nm, (ii) w = 0.55–1.5 nm, (iii) w = 1.5–3.0 nm and (iv) w > 3.0 nm according to the solvated electrolyte ion size (Figure 4). Li ions in LiClO$_4$/PC solution form Li$^+$-4PCs in bulk phase whose diameter is ~1.4 nm[46]. The first domain (w < 0.55 nm) corresponds to the size of short axis of a PC molecule; even PC molecules are considered impossible to access into the pore. In the second domain (w = 0.55–1.5 nm), the solvated ions barely access into the pore as long as desolvation is occurred. In the third domain (w = 1.5–3.0 nm), the solvated ions smoothly access into the pore without desolvation. In last domain (w > 3.0 nm), the solvated ions can form EDLs on each pore wall, whose schematic images are illustrated in Supplementary Information Fig. S7. The T1 and A1 microporous carbons are composed chiefly of pores with w < 1.5 nm (Fig. 4(a)), showing extremely low gravimetric and area-specific capacitances. Micropores in them should connect not to large spaces whose pore size is above the solvated ion size, but rather connect directly to external surface. It implies that the large spaces connected to micropores where solvated ions can access needs for effective use of micropores to improve EDL capacitance. Such slightly large spaces against the solvated ion should facilitate desolvation because of a strong interaction field. When dominant pores are micropores of w < 1.5 nm, the area-specific capacitance is low even on the WL-shape carbon. The M1 carbon provides high gravimetric capacitance but quite low area-specific capacitance. The high gravimetric capacitance

of M1 carbon stems from the high specific surface area above 2000 m^2/g; however, the low area-specific capacitance suggests that the micropore surface hardly contributes the EDL formation. It is similar reason with the slit-shape microporous carbons. Other slit-shape carbons have large amount of mesopores, but the gravimetric capacitance is lower than PorC18. On the micro/mesoporous slit-shape carbons with large specific surface area, the larger surface area they have, the lower area-specific capacitance is; the electrode surface in slit-shape carbon even with mesopores should not be worked effectively. On the other hand, the WL-shape carbons except for the microporous M1 carbon provide high gravimetric and area-specific capacitances.

The unique property of WL-shape carbons has been clarified by investigating the ratio of surface area of interconnected pores (Figure 5). The ratio of specific surface area (R_{ssa}) was given by the surface area with $w > 1.5$ nm ($S_{w>1.5}$) divided by the surface area with $w = 0.55–1.5$ nm ($S_{w=0.55–1.5}$); $R_{ssa} < 1$ represents that a dominant space is not for solvated ions but for desolvated ions. As the PorC-type carbons are composed predominantly of mesopores consisting of crooked pore walls, here, they fall into the same category as the WL-shape carbon. In the case of slit-shape carbon, the gravimetric capacitance increases towards $R_{ssa} = 1$. It reaches the same value of WL-shape mesoporous carbons. Each relationship between the gravimetric capacitance and the surface areas ($S_{w>1.5}$ and $S_{w=0.55–1.5}$) also clearly shows the effect of spaces for solvated/desolvated ions on the gravimetric capacitance (See Supplementary Information Fig. S8). Although the gravimetric capacitance of slit-shape carbons proportionally increases with increasing $S_{w>1.5}$ (Fig. S8(b)), the capacitance does not depend on the surface area with $w = 0.55–1.5$ nm (Fig. S8(a)). It suggests that spaces for desolvated ions in the slit-shape carbon nearly defunct on providing EDL capacitance. On the other hand, the gravimetric capacitance of WL-shape carbons with $R_{ssa} \leq 1$ is larger than that of mesoporous carbons with $R_{ssa} > 1$. The contribution of spaces for desolvated ions in WL-shape carbons to gravimetric capacitance is also shown in Fig. S8(a). The gravimetric capacitance increases with the increasing the value of surface area with $w = 0.55$-1.5 nm until ~1100 m^2/g and then decreases. Such low gravimetric capacitance at the large specific surface area implies that most of the spaces for desolvated ions do not contribute to the EDL formation even in WL-shape carbon. The gravimetric capacitance against $R_{ssa} < 0.5$ is thus decreased. The availability of spaces with $w = 0.55$-1.5 nm must depend strongly on the spaces with $w > 1.5$ nm connecting the smaller pores. The desolvation is accelerated by the strong confinement effect from the spaces with $w > 1.5$ nm, and the desolvated ions frequently pass through the smaller pores. The WL-shape carbons (M2 and M3) thus show anomalous high EDL capacitance compared with previous reports (See Supplementary Information Fig. S9). The carbon samples providing high EDL capacitance in the previous reports have very high specific surface area (~3000 m^2/g). On the other hands, the M2 and M3 carbon samples can provide high EDL capacitance above 200 F/g despite small surface area (~1800 m^2/g). The relationship between the gravimetric capacitance

and the ratio of value of specific surface area demonstrates that R_{ssa} ~0.5 is ideal ratio of pores for solvated and desolvated ions to improve EDL capacitance.

Conclusions

In summary, our findings show that the ratio of surface area of the pores with desolvated ion size and the solvated ion size as well as pore the shape is quite important to design porous carbon electrodes providing extremely high EDL capacitance. The 15 different porous carbons with similar amount of defective sites have been broadly classified according to the pore shapes determined from the direct observation of carbon framework and the comparison of plane size. The micro/mesoporous carbons categorized into the WL-shape demonstrate higher EDL capacitance than the slit-shape carbons. More in-depth analysis of porous structures proposed new factor to design porous carbon electrodes. The ratio of spaces (R_{ssa}), where solvated/desolvated ions access, profoundly affects the EDL capacitances, and the results indicate an ideal structure is a hierarchical porous structure with R_{ssa} ~0.5 and WL-shape pores. We believe that the structural factors shown in this study will be successfully applied even in other electrolytes and will facilitate modelling of high capacitance EDLC electrodes.

Notes and references

1.   Z. Niu, L. Liu, L. Zhang, W. Zhou, X. Chen and S. Xie, *Adv. Energy Mater.*, 2015, **5**, 1500677.
2.   Z. Liu, Z. S. Wu, S. Yang, R. Dong, X. Feng and K. Mullen, *Adv. Mater.*, 2016, **28**, 2217-2222.
3.   P. Huang, C. Lethien, S. Pinaud, K. Krousse, R. Laloo, V. Turq, M. Respaud, A. Demortière, B. Daffos, P. L. Taberna, B. Chaudret, Y. Gogotsi and P. Simon, *Science*, 2016, **351**, 691-695.
4.   I. Moriguchi, *Chem. Lett.*, 2014, **43**, 740-745.
5.   A. B. Fuertes, G. Lota, T. A. Centeno and E. Frackowiak, *Electrochim. Acta*, 2005, **50**, 2799-2805.
6.   T. Ohkubo, T. Iiyama, K. Nishikawa, T. Suzuki and K. Kaneko, *J. Phys. Chem. B*, 1999, **103**, 1859-1863.
7.   T. Ohkubo, T. Konishi, Y. Hattori, H. Kanoh, T. Fujikawa and K. Kaneko, *J. Am. Chem. Soc.*, 2002, **124**, 11860-11861.
8.   J. Imai, M. Souma, S. Ozeki, T. Suzuki and K. Kaneko, *J. Phys. Chem.*, 1991, **95**, 9955-9960.
9.   M. Miyahara and K. E. Gubbins, *J. Chem. Phys.*, 1997, **106**, 2865-2880.
10.   S. Hashimoto, T. Fujimori, H. Tanaka, K. Urita, T. Ohba, H. Kanoh, T. Itoh, M. Asai, H. Sakamoto, S. Niimura, M. Endo,

F. Rodriguez-Reinoso and K. Kaneko, *J. Am. Chem. Soc.*, 2011, **133**, 2022-2024.

11. K. Urita, Y. Shiga, T. Fujimori, T. Iiyama, Y. Hattori, H. Kanoh, T. Ohba, H. Tanaka, M. Yudasaka, S. Iijima, I. Moriguchi, F. Okino, M. Endo and K. Kaneko, *J. Am. Chem. Soc.*, 2011, **133**, 10344-10347.

12. B. Coasne, Y. Long and K. E. Gubbins, *Mol. Simul.*, 2014, **40**, 721-730.

13. J. Chmiola, G. Yushin, Y. Gogotsi, C. Portet, P. Simon and P. L. Taberna, *Science*, 2006, **313**, 1760-1763.

14. E. Raymundo-Piñero, K. Kierzek, J. Machnikowski and F. Béguin, *Carbon*, 2006, **44**, 2498-2507.

15. H. Wang, T. K. J. Köster, N. M. Trease, J. Ségalini, P.-L. Taberna, P. Simon, Y. Gogotsi and C. P. Grey, *J. Am. Chem. Soc.*, 2011, **133**, 19270-19273.

16. C. Merlet, C. Pean, B. Rotenberg, P. A. Madden, B. Daffos, P. L. Taberna, P. Simon and M. Salanne, *Nat. Commun.*, 2013, **4**, 2701.

17. T. Ohba and K. Kaneko, *J. Phys. Chem. C*, 2013, **117**, 17092-17098.

18. W. Y. Tsai, P. L. Taberna and P. Simon, *J. Am. Chem. Soc.*, 2014, **136**, 8722-8728.

19. A. C. Forse, C. Merlet, J. M. Griffin and C. P. Grey, *J. Am. Chem. Soc.*, 2016, **138**, 5731-5744.

20. R. M. Burt, K. K. Breitsprecher, B. Daffos, P. L. Taberna, P. Simon, G. Birkett, X. S. Zhao, C. Holm and M. Salanne, *J. Phys. Chem. Lett.*, 2016, **7**, 4015-4021.

21. M. Salanne, B. Rotenberg, K. Naoi, K. Kaneko, P. L. Taberna, C. P. Grey, B. Dunn and P. Simon, *Nat. Energy*, 2016, **1**, 16070.

22. K. Urita, N. Ide, K. Isobe, H. Furukawa and I. Moriguchi, *ACS Nano*, 2014, **8**, 3614-3619.

23. A. Garcia-Gomez, G. Moreno-Fernandez, B. Lobato and T. A. Centeno, *Phys. Chem. Chem. Phys.*, 2015, **17**, 15687-15690.

24. N. Jäckel, M. Rodner, A. Schreiber, J. Jeongwook, M. Zeiger, M. Aslan, D. Weingarth and V. Presser, *J. Power Sources*, 2016, **326**, 660-671.

25. N. Jäckel, P. Simon, Y. Gogotsi and V. Presser, *ACS Energy Lett.*, 2016, **1**, 1262-1265.

26. D. Lozano-Castelló, M. A. Lillo-Ródenas, D. Cazorla-Amorós and A. Linares-Solano, *Carbon*, 2001, **39**, 741-749.

27. C. Portet, Z. Yang, Y. Korenblit, Y. Gogotsi, R. Mokaya and G. Yushin, *J. Electrochem. Soc.*, 2009, **156**, A1.

28. L. Wei, M. Sevilla, A. B. Fuertes, R. Mokaya and G. Yushin, *Adv. Energy Mater.*, 2011, **1**, 356-361.

29. L. Wei and G. Yushin, *Nano Energy*, 2012, **1**, 552-565.

30. S. Kumagai, M. Sato and D. Tashima, *Electrochim. Acta*, 2013, **114**, 617-626.

31. B. E. Conway, V. Briss and J. Wojtowixz, *J. Power Sources*, 1997, **66**, 1-14.

32. H. Oda, A. Yamashita, S. Minoura, M. Okamoto and T. Morimoto, *J. Power Sources*, 2006, **158**, 1510-1516.

33. S. Aono, T. Tsurudo, K. Urita and I. Moriguchi, *Chem. Commun.*, 2013, **49**, 2939-2941.

34. I. Moriguchi, F. Nakahara, H. Furukawa, H. Yamada and T. Kudo, *Electrochem. Solid-State Lett.*, 2004, **7**, A221-A223.

35. M. Okoshi, Y. Yamada, A. Yamada and H. Nakai, *J. Electrochem. Soc.*, 2013, **160**, A2160-A2165.

36. L. Hu, D. Guo, G. Feng, H. Li and T. Zhai, *J. Phys. Chem. C*, 2016, **120**, 24675-24681.

37. A. C. Ferrari and J. Robertson, *Phys. Rev. B*, 2000, **61**, 14095-14107.

38. A. C. Ferrari and J. Robertson, *Phys. Rev. B*, 2001, **64**, 075414.

39. M. S. Dresselhaus, A. Jorio, A. G. Souza Filho and R. Saito, *Philos. Trans. R. Soc. London, Ser. A*, 2010, **368**, 5355-5377.

40. Y. Kobayashi, K.-i. Fukui, T. Enoki and K. Kusakabe, *Phys. Rev. B*, 2006, **73**, 125415.

41. M. T. Miyahara, R. Numaguchi, T. Hiratsuka, K. Nakai and H. Tanaka, *Adsorption*, 2013, **20**, 213-223.

42. G. Salitra, A. Soffer, L. Eliad, Y. Cohen and D. Aurbach, *J. Electrochem. Soc.*, 2000, **147**, 2486-2493.

43. M. Hahn, M. Baertschi, O. Barbieri, J. C. Sauter, R. Kötz and R. Gallay, *Electrochem. Solid-State Lett.*, 2004, **7**, A33.

44. C. Portet, G. Yushin and Y. Gogotsi, *Carbon*, 2007, **45**, 2511-2518.

45. J. Huang, B. G. Sumpter, V. Meunier, G. Yushin, C. Portet and Y. Gogotsi, *J. Mater. Res.*, 2011, **25**, 1525-1531.

46. H. Ohtani, Y. Hirao, A. Ito, K. Tanaka and O. Hatozaki, *J. Therm. Anal. Calorim.*, 2010, **99**, 139-144.

Supplementary Information

**Ideal Porous Structure of EDLC Carbon Electrode with Extremely High Capacitance**

K. Urita,[a][*] C. Urita,[a] K. Fujita,[a] K. Horio,[b] M. Yoshida[b] and I. Moriguchi[a]

[a] Graduate School of Engineering, Nagasaki University, 1-14 Bunkyo-machi, Nagasaki, Nagasaki 852-8521, Japan.

[b] MicrotracBEL Corp., 8-2-51 Nankohigashi, Suminoe-ku, Osaka 559-0031, Japan.

*Corresponding Author: urita@nagsaki-u.ac.jp
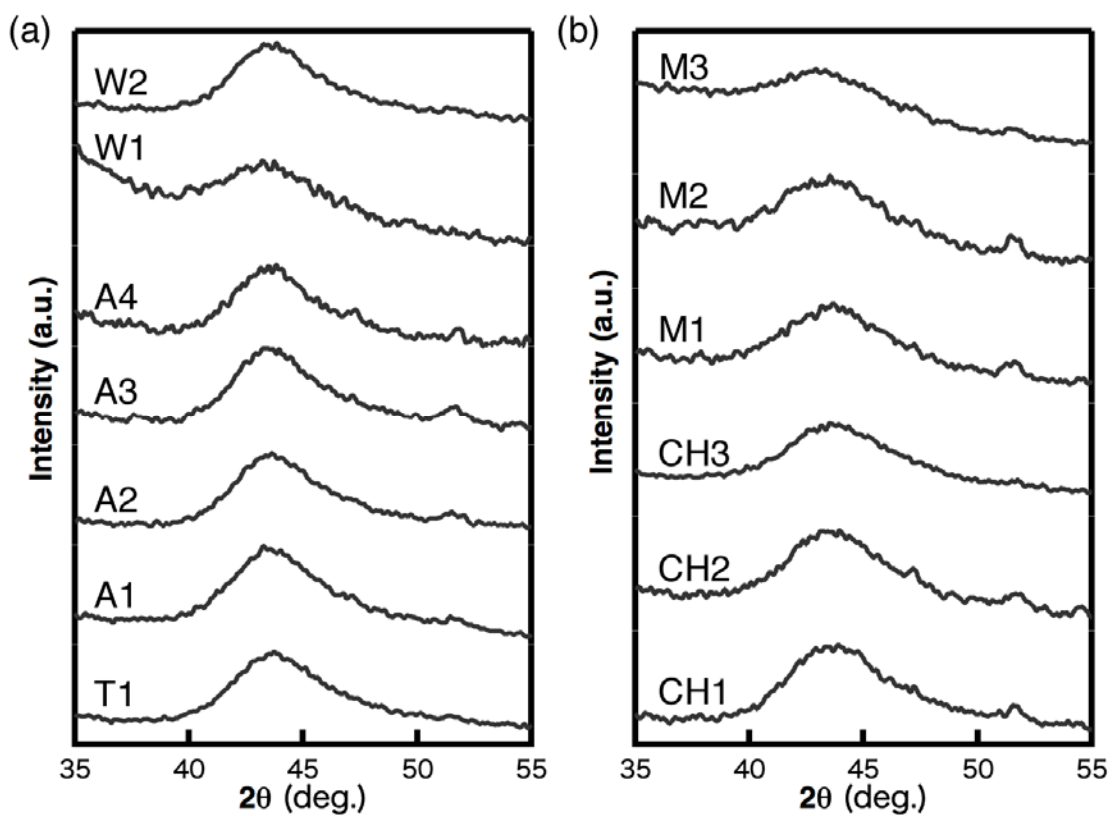
Figure S1. XRD patterns of (a) slit-shape carbon and (b) WL-shape carbon relevant to (10) plane in graphitic structure.
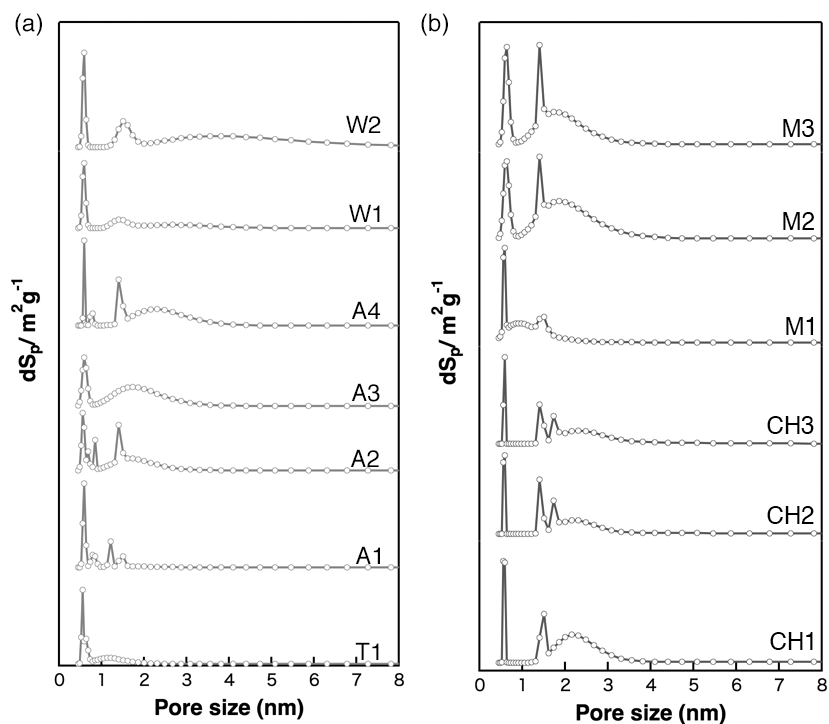
Figure S2. Pore size distribution of (a) slit-shape carbon and (b) WL-shape carbon.

Table S1 Specific surface area of each sample determined from GCMC method. The unit of surface areas is m^2/g.

Sample	Micropore	Mesopore	Macropore	Total
T1	1031	4		1035
A1	1124	11		1135
A2	1271	132		1403
A3	1167	288	0	1455
A4	1168	588		1756
W1	786	116		902
W2	710	342		1052
CH1	796	406		1202
CH2	774	239		1013
CH3	702	297		999
M1	2222	57	0	2279
M2	1353	430		1783
M3	1499	297		1796
PorC18	656	666	15	1337
PorC45	482	411	81	974
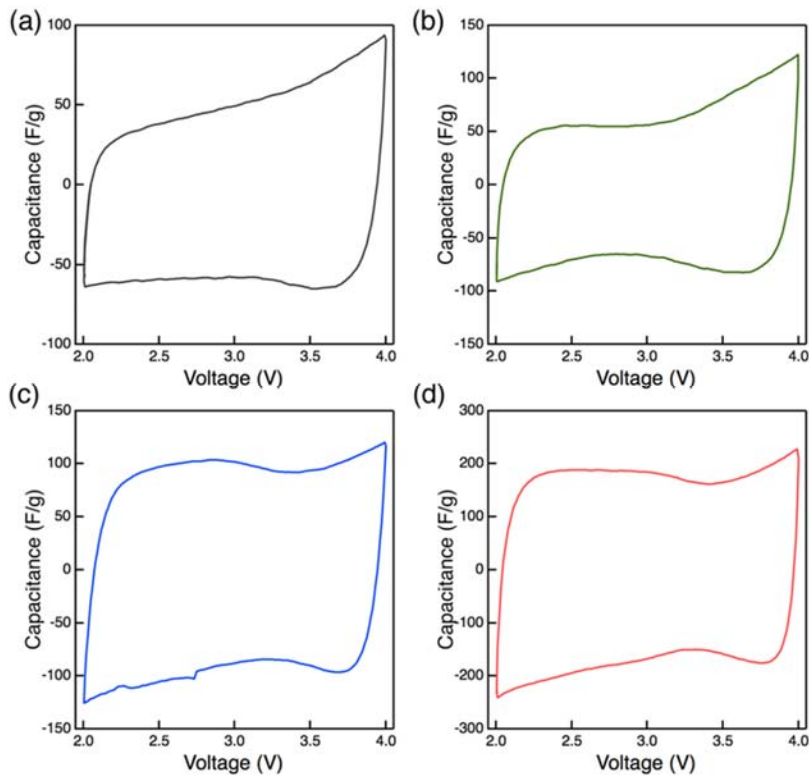
Figure S3. CV curves of representative porous carbon samples, (a) W1 and (b) A4 in the slit-shape and (c) CH2, (d) M3 in the WL-shape.
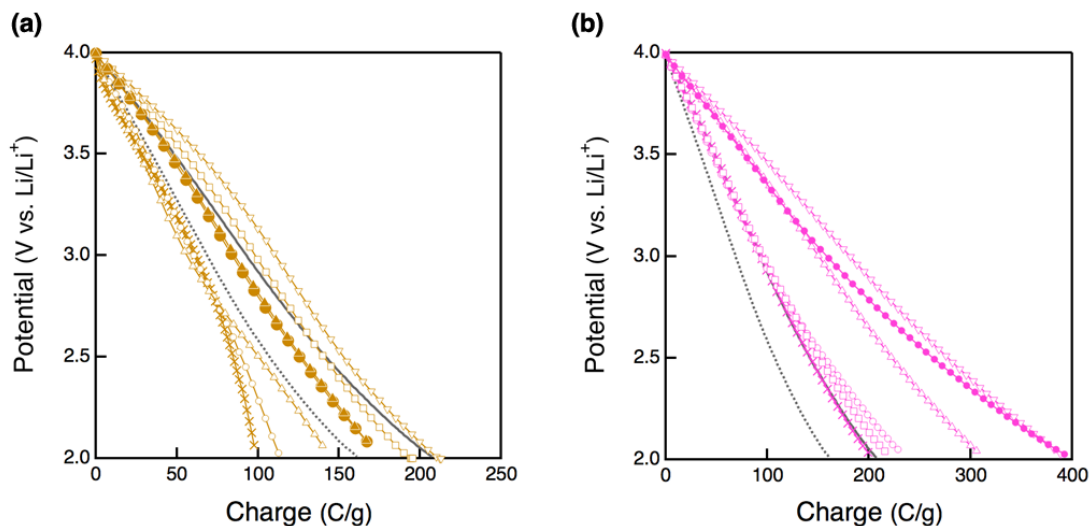

Figure S4. 3rd discharge curves obtained in the CC mode at a current density of 10 mA/g for the slit-shape carbon (Cross, T1; open circle, A1; open square, A2; open triangle, A3; open inverted triangle, A4; closed circle, W1; closed triangle, W2) in (a) and the WL-shape carbon (Cross, CH1; open circle, CH2; open square, CH3; open triangle, M1; open inverted triangle, M2; closed circle, M3) in (b). The grey thin line and dotted line in (a) and (b) are curves of PorC18 and PorC45, respectively.
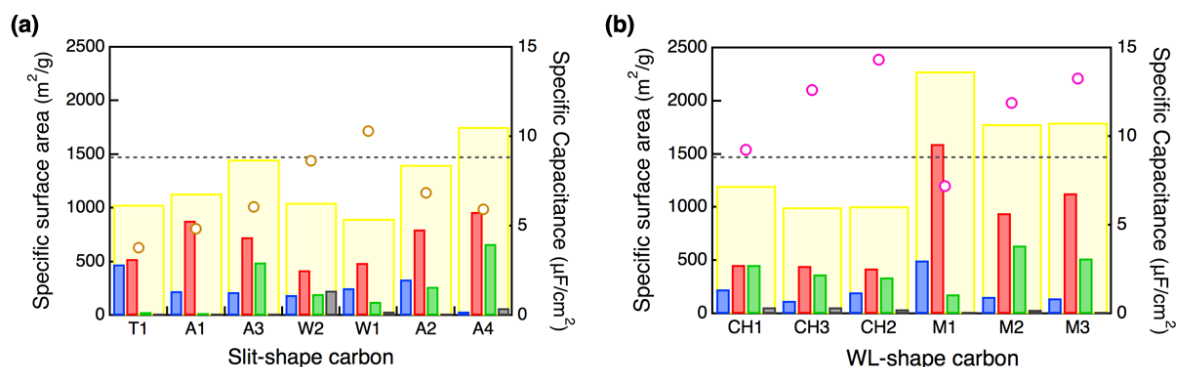
Figure S5. Specific surface area with pore size of < 0.55 nm (blue), 0.55–1.5 nm (red), 1.5–3.0 nm (green), > 3.0 nm (black) and total specific surface area (yellow),and area-specific capacitance at the current density of 10 mA/g (ocher in (a) and pink in (b)) on the slit-shape carbon (a) and WL-shape carbon (b). Grey short-broken lines reveal the area-specific capacitance (8.8 µF/cm^2) of PorC18.
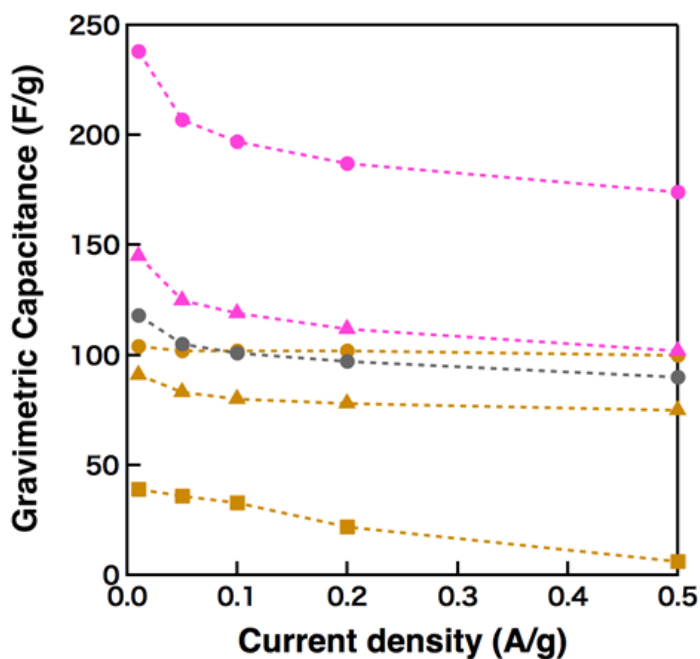

Figure S6. Rate performance of representative porous carbon samples (Pink closed circle, M3; closed triangle, CH2; Grey closed circle, PorC18; Ocher closed circle, A4; closed triangle, W2; closed square, T1).
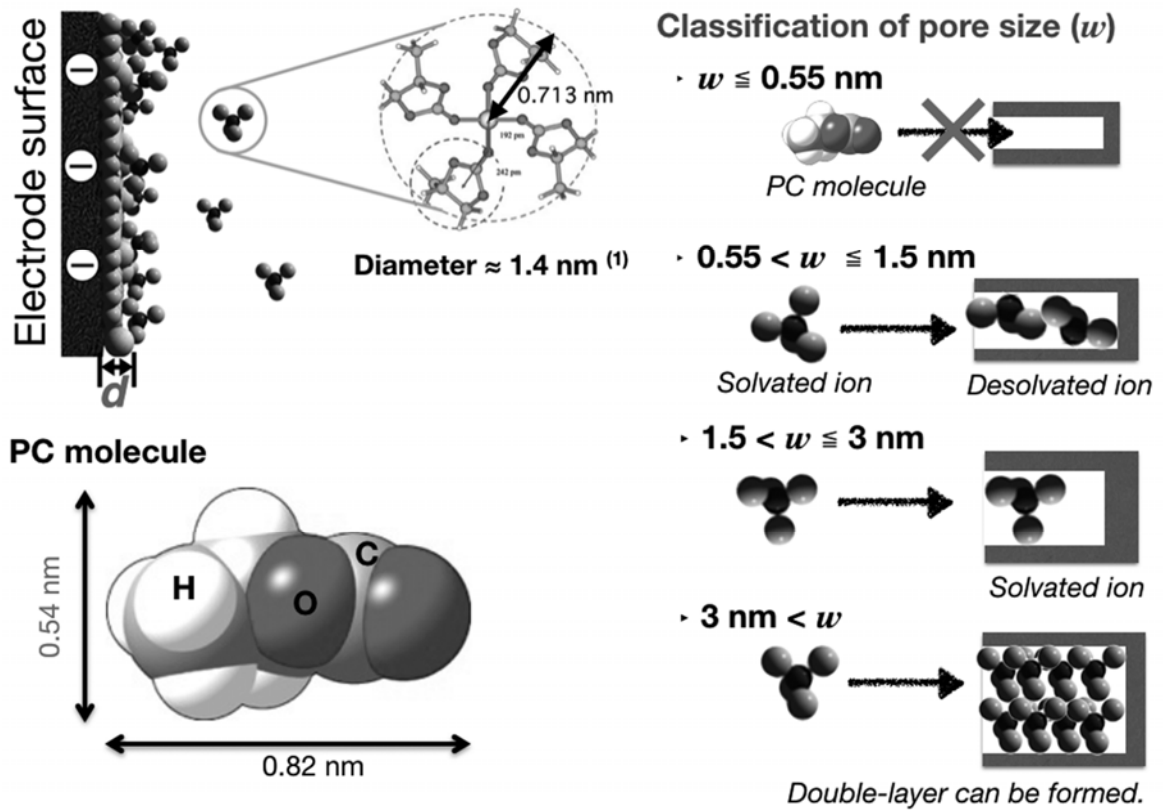
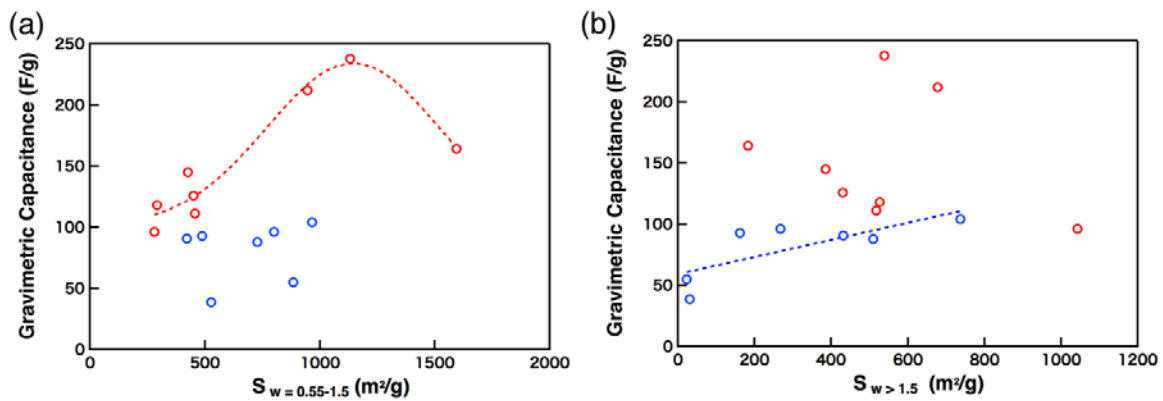**Figure S7 Schematic images relevant to solvated ion size and pore size.**

Figure S8. Relationship between the gravimetric capacitance and specific surface area with *w* = 0.55–1.5 nm (a) and > 1.5 nm (b) on slit-shape (blue) and WL-shape (red) carbons.
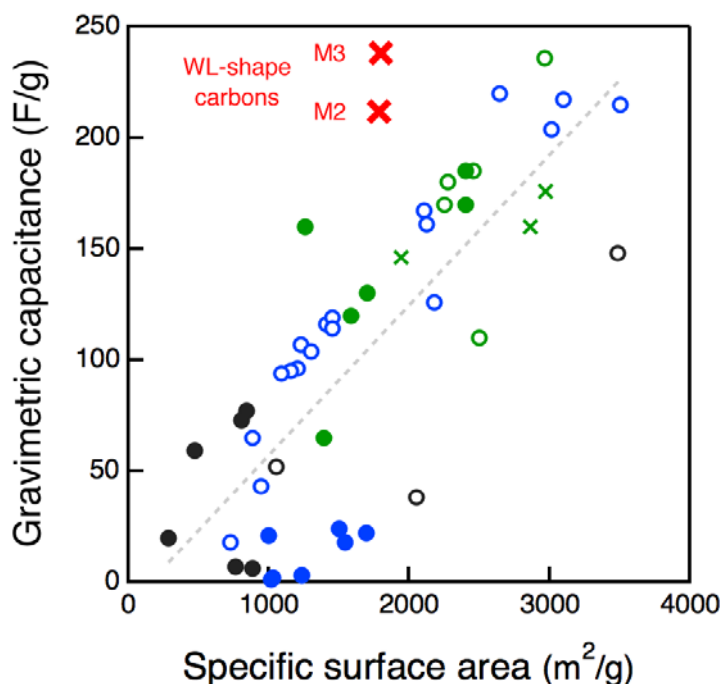
Figure S9. Gravimetric capacitance vs. specific surface are plots of our WL-shape carbons with R_{ssa} = 0.5 (M3) and R_{ssa} = 0.7 (M2) as well as the reported carbons (Blue open circle, activated carbons[2,3]; closed circle, mesoporous carbons[4] in LiClO$_4$/PC; Green open circle, activated carbons[5-7]; closed circle, carbide-derived carbons[8-11]; cross, zeolite-templated carbons[12-15] in TEABF$_4$/AN; Gray open circle, activated carbons[16-18]; closed circle, aerogel-derived carbons[19] in TEABF$_4$/PC).

Supporting references
(1) H. Ohtani, Y. Hirao, A. Ito, K. Tanaka, O. Hatozaki, *J. Therm. Anal. Calorim.* 99(1) (2010) 139.
(2) M. Endo, T. Maeda, T. Takeda, Y. J. Kim, K. Koshiba, H. Hara, M. S. Dresselhaus, *J. Electrochem. Soc.* 148 (2001) A910.
(3) D. L-Castello, D. C-Amoróa, A. L-Solano, S. Shiraishi, H. Kurihara, A. Oya, *Carbon* 41 (2003) 1765.
(4) H. Yamada, I. Moriguchi, T. Kudo, *J. Power Sources* 175 (2008) 651.
(5) P. Azaïs, L. Duclaux, P. Florian, D. Maasiot, M. A. L-Rodenas, A. L-Solano, J-P. Peres, C. Jehoulet, F. Beguin, *J. Power Sources* 171 (2007) 1046.
(6) Y. Korenblit, M. Rose, E. Kockrick, L. Borchardt, A. Kvit, S. Kaskel, G. Yushin, *ACS Nano* 4 (2010) 1337.
(7) L. Wei, M. Sevilla, A. B. Fuertes, R. Mokaya, G. Yushin, *Adv. Energy Mater.* 1 (2011) 356.
(8) J. Chmiola, G. Yushin, Y. Gogotsi, C. Portet, P. Simon, *Science* 313 (2006) 1760.
(9) R. K. Dash, J. Chmiola, G. Yushin, Y. Gogotsi, G. Laudisio, J. Singer, J. FIscher, S. Kucheyev, *Carbon* 44 (2006) 2489.
(10) M. Arulepp, J. Leis, M. Latt, F. Miller, K. Rumma, E. Lust, A. F. Burke, *J. Power Sources* 162 (2006) 1460.
(11) V. Presser, L. F. Zhang, J. J. Niu, J. McDonough, C. Perez, H. Fong, Y. Gogotsi, *Adv. Energy Mater.* 1 (2011) 423.
(12) H. L. Wang, Q. M. Gao, J. Hu, Z. Chen, *Carbon* 47 (2009) 2259.
(13) C. Portet, Z. Yang, Y. Korenblit, Y. Gogotsi, R. Mokaya, G. Yushin, *J. Electrochem. Soc.* 156 (2009) A1.
(14) H. L. Wang, Q. M. Gao, J. Hu, *Microporous Mesoporous Mater.* 131 (2010) 89.
(15) H. Itai, H. Nishihara, T. Kogure, T. Kyotani T, *J. Am. Chem. Soc*. 133 (2011) 1165.
(16) H. Yang, M. Yoshio, K. Isono, R. Kuramoto, *Electrochem. Solid-State Lett.* 5 (2002) A141.
(17) Y. J. Kim, Y. Horie, S. Ozaki, Y. Matsuzawa, H. Suezaki, C. Kim, N. Miyashita, M. Endo, *Carbon* 42 (2004) 1491.
(18) D. H-Jurcakova, M. Kodama, S. Shiraishi, H. Hatori, Z. H. Zhu, G. Q. Lu, *Adv. Funct. Mater.* 19 (2009) 1800.
(19) B. Szubsda, A. Szmaja, A. Halama, *Electrochim. Acta* 86 (2012) 255.